Hindawi
Advances in Materials Science and Engineering
Volume 2023, Article ID 9790582, 1 page
https://doi.org/10.1155/2023/9790582

Retraction

Retracted: A Study of Structural Parameters Effects on Pressure Differential to Roll Titanium Diaphragm for a Spacecraft Propellant Tank

Advances in Materials Science and Engineering

Received 26 December 2023; Accepted 26 December 2023; Published 29 December 2023

This article has been retracted by Hindawi, as publisher, following an investigation undertaken by the publisher [1]. This investigation has uncovered evidence of systematic manipulation of the publication and peer-review process. We cannot, therefore, vouch for the reliability or integrity of this article.

Please note that this notice is intended solely to alert readers that the peer-review process of this article has been compromised.

Wiley and Hindawi regret that the usual quality checks did not identify these issues before publication and have since put additional measures in place to safeguard research integrity.

We wish to credit our Research Integrity and Research Publishing teams and anonymous and named external researchers and research integrity experts for contributing to this investigation.

The corresponding author, as the representative of all authors, has been given the opportunity to register their agreement or disagreement to this retraction. We have kept a record of any response received.

References

[1] T. Ma, S. Gu, J. Zhao, B. Yu, J. Zhang, and W. Yang, "A Study of Structural Parameters Effects on Pressure Differential to Roll Titanium Diaphragm for a Spacecraft Propellant Tank," *Advances in Materials Science and Engineering*, vol. 2022, Article ID 2003905, 10 pages, 2022.

Hindawi
Advances in Materials Science and Engineering
Volume 2022, Article ID 2003905, 10 pages
https://doi.org/10.1155/2022/2003905

Research Article

A Study of Structural Parameters Effects on Pressure Differential to Roll Titanium Diaphragm for a Spacecraft Propellant Tank

Tianju Ma, Sendong Gu, Jipeng Zhao, Bin Yu, Jianjun Zhang, and Wenbo Yang

Science and Technology on Vacuum Technology and Physics Laboratory, Lanzhou Institute of Physics, Lanzhou 730000, China

Correspondence should be addressed to Sendong Gu; cast510_gsd@163.com

Received 22 June 2022; Accepted 3 October 2022; Published 8 November 2022

Academic Editor: K. Raja

A range of titanium diaphragms for spacecraft propellant tanks are designed in detail, and two typical titanium diaphragms were manufactured and corresponding reversal tests were developed. A series of finite element models of the reversal process of these titanium diaphragms is developed based on the arc-length method and a finite element analysis software. With the aid of the models, this paper analyzes the characteristics of pressure drop during the whole reversal process and investigates the effects of the structural parameters on pressure differential to roll titanium diaphragm. The results show that simulated values of the critical pressure and the overturning pressure show good agreement with measured ones. In addition, the critical pressure increases with increasing thickness, decreasing bottom diameter and chamfering radius. The thickness and the bottom diameter are the main influence factors for the critical pressure. The overturning pressure increases with increasing thickness and arc radius. These effects of the bottom diameter, the chamfering radius, and arc radius become sharper with increasing thickness.

1. Introduction

Diaphragm tanks are one of the most practical positive expulsion devices, which are extensively used in spacecraft propellant systems. The devices are capable to store and manage common liquid propellants, when the station keeping, orbit, and altitude control for spacecrafts are carried out. In most cases, a diaphragm tank mainly consists of four components, including a top hemispherical shell, a diaphragm, a bottom hemispherical shell, and a retaining ring. Its working principle is shown in Figure 1. The top and bottom hemispherical shells can suffer a certain internal pressure. The diaphragm separates the internal chamber of the two hemispherical shells into two parts as a barrier, including a gas chamber and a liquid chamber when the tank contains a liquid propellant. The diaphragm will be rolled by pressure differential between the two chambers, and the propellant will be expelled from its storage chamber subsequently.

The diaphragm is the key component of the tank. In the past, most of them are made from a thin material with better ductility, such as rubber materials, which are flexible enough to couple to the internal surface of the shell and adjust the shape at all fill-levels. Some works [1–6] have been performed on the spacecraft propellant tanks with rubber diaphragms. However, the common propellants like hydrazine, MMH, and N_2O_4 are not compatible with the rubber materials [7–9]. As of recent, in order to meet the requirement of long-term propellant storage, the focus of research has been on the feasibility of metallic diaphragms, including titanium diaphragms and aluminum diaphragms [10]. Lenahen et al. [11] investigated the liquid slosh behaviors in spacecraft propellant tanks with metal diaphragms by computational and experimental analysis. Conomos et al. [8] and Marvih et al. [12] developed a titanium tank and aluminum diaphragm tanks, respectively, the motions of these diaphragms were also characterized. Instead of conventional rubber diaphragms, the plastic deformation is dominant during the reversal process [8, 13]. As a key parameter for guiding structural design, the pressure differential to roll the metal diaphragm is affected by its structural parameters complexly. Therefore, further studies on the effects are still essential.

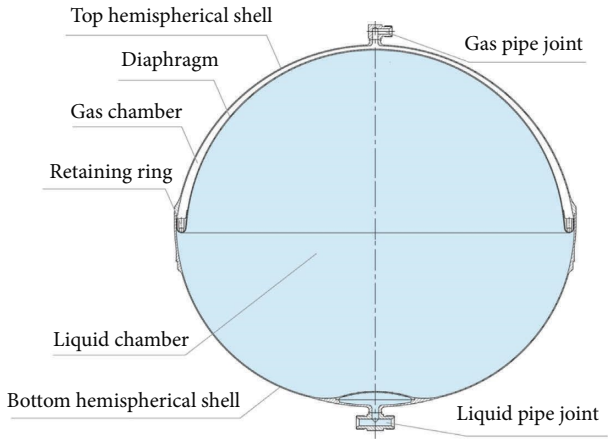

Figure 1: Schematic diagram of a diaphragm tank.

In this work, a range of titanium diaphragms are designed in detail. The effects of structural parameters on pressures differential to roll these diaphragms are investigated by combining the method of experimental observation, numerical simulation, and theoretical analysis.

2. Titanium Diaphragm Structure and Experimental Setup

2.1. Titanium Diaphragm Structure. The titanium alloy used in this investigation is TA1ELI, which is a titanium-based alloy. Its chemical composition is given in Table 1. As the basic structure of a common titanium diaphragm is shown in Figure 2, the diaphragm is a thin shell structure, where thickness increases from the bottom to the top. A chamfering structure is set up as a flanging section at the bottom of the diaphragm to mount the retaining ring. An arc section is employed to fit the interior shape of the top hemispherical shell. In order to deform steadily at the beginning of reversal process, a cone section is designed between the flanging section and the arc section. The structural parameters for the diaphragm, such as the thickness, T, the bottom diameter, D_b, the chamfering radius, R_f, the arc radius, R_a, the height, H, and the angle of cone section, α are significant [14–17], which affect the service properties of the diaphragm, especially the pressure drop. In general, H is limited by the height of tanks and α is defined as a constant to simplify the design. So the effects of key structural parameters, including T, D_b, R_f ,and R_a are studied in this work. Two typical titanium diaphragms were designed and manufactured, and key structural parameters are listed in Table 2.

2.2. Diaphragm Reversal Tests. In order to investigate the performance of the titanium diaphragm experimentally, reversal tests were developed. Figure 3 illustrates a schematic diagram of the test process. Before test, the gas pipe joint of the tank was connected to a gas pressure controller via a buffer vessel. Then, water was replaced for hydrazine propellant due to similar liquid specifications [18–20] to be filled into the liquid chamber from the liquid pipe joint.

Table 1: Chemical composition of TA1ELI (wt (%)).

Fe	Si	C	N	H	O
≤0.05	0.01	≤0.10	0.003	0.0008	0.035

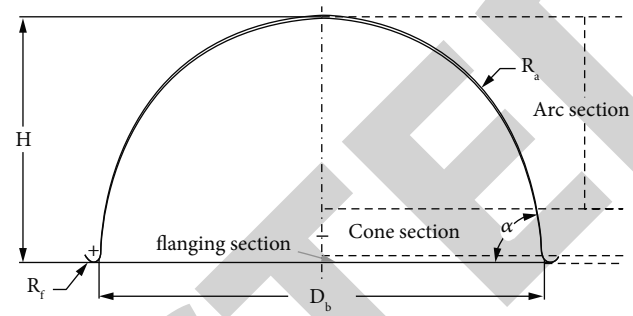

Figure 2: Basic structure of a common titanium diaphragm.

Subsequently, a pressure differential transducer was placed and measured the pressure differential between the gas chamber and the liquid chamber. The pressure differential and the corresponding volumetric change of the liquid chamber were measured at a base gas pressure of 0.02 MPa until the final gas pressure of 0.5 MPa was obtained. Figure 4 provides the initial titanium diaphragms and the deformed ones when rolled fully.

3. Finite Element Simulation Setup

In order to investigate the effects of the structural parameters on pressure differential, finite element (FE) models of the reversal process of all the designed titanium diaphragms are developed based on the arc-length method and a FE analysis software. This part concentrates on the procedure of simulation development. The validity of the FE models is verified by the above experimental results.

3.1. Diaphragm Geometries. Except for the above two designed diaphragms, a range of titanium diaphragms are designed in detail. These diaphragms can be divided into four broad groups based on their interior dimensions as shown in Figure 5. The dimensions of the thickness, T and the chamfering radius, R_f for every group are listed in Table 3. It means that there are 12 designed titanium diaphragms for every group.

3.2. Theoretical Approach. The deformation of metal diaphragms during the reversal process is a complex nonlinear structural response with strain softening, which is characterized by the drop of stress after achieving the peak value. In this case, nonlinear FE analysis is likely to suffer from convergence issues [21, 22]. To overcome this problem, the so-called arc-length method has been proposed and developed by numerous researchers [23, 24] to compute complex equilibrium paths in nonlinear structural mechanics problems.

Table 2: Key structural parameters of two diaphragms.

Serial number	T (mm)			D_b (mm)	R_f (mm)	R_a (mm)
	Flanging section	Cone section	Arc section			
E1	1.00	1.00	1.00–1.50	433.4	5	216.0
E2	1.00	1.00	1.00–1.50	599.4	6	278.7

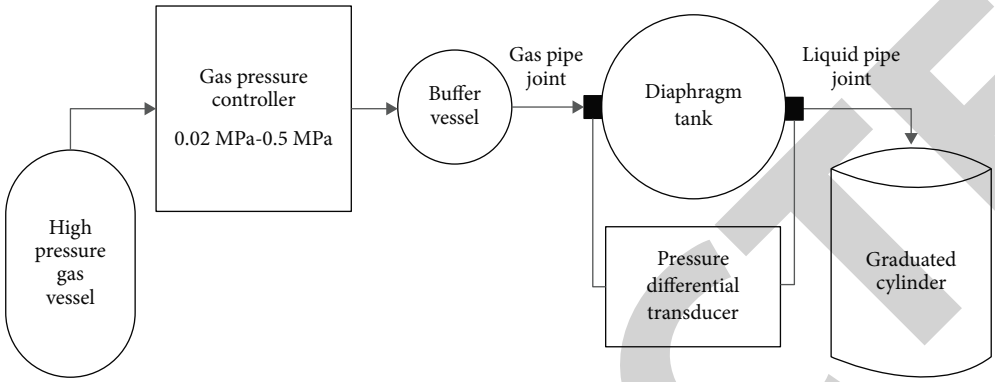

Figure 3: Schematic diagram of the reversal test process.

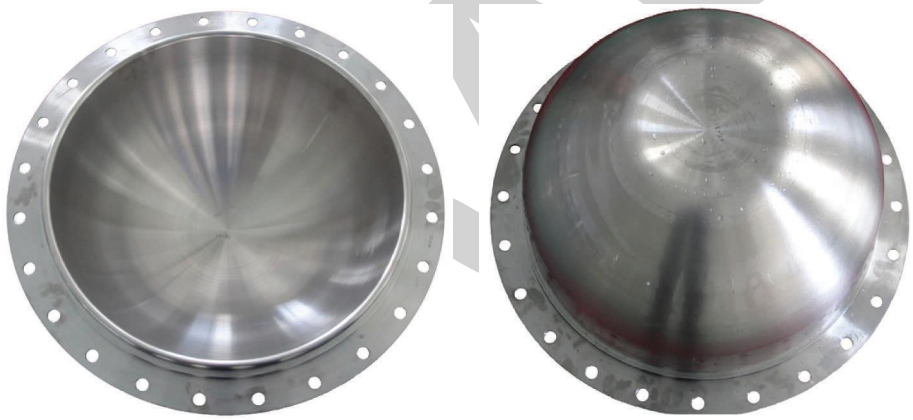

Figure 4: Initial titanium diaphragm (a) and the deformed ones when rolled fully (b).

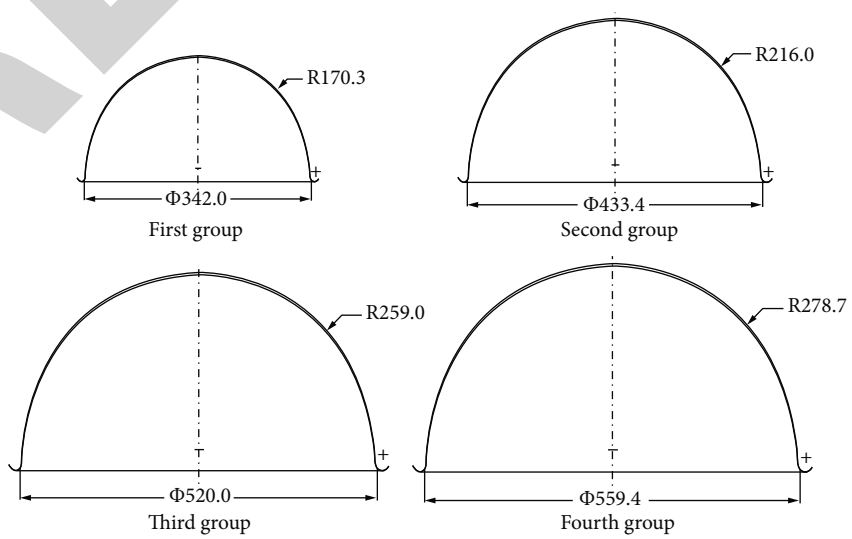

Figure 5: Interior dimensions of titanium diaphragms for every group.

Table 3: Dimensions of the thickness, T and the chamfering radius, R_f for every group.

T (mm)			R_f (mm)
Flanging section	Cone section	Arc section	
0.40	0.40	0.56–0.60	5, 6, 7
0.60	0.60	0.84–0.90	5, 6, 7
0.80	0.80	1.12–1.20	5, 6, 7
1.00	1.00	1.40–1.50	5, 6, 7

When adapting the FE method for computing numerical solutions, the approximation of the nonlinear structural mechanics problem can be expressed as follows:

$$\mathbf{R}(u,\lambda) = \mathbf{F}_{\text{int}}(u) - \lambda \mathbf{F}_{\text{ext}} = 0. \tag{1}$$

Here $\mathbf{R}$ has been defined as the residual vector, $\boldsymbol{u}$ is the nodal displacement vector, λ is the load factor, $\mathbf{F}_{\text{int}}(\boldsymbol{u})$ and $\mathbf{F}_{\text{ext}}$ denote the internal force vector and the external force vector, respectively.

Generally, equation (1) is solved by means of an incremental approach. So the nodal displacement vector $\boldsymbol{u}_{n+1}$ and the load factor λ_{n+1} at the current load step are defined as:

$$u_{n+1} = u_n + \Delta u, \tag{2}$$

$$\lambda_{n+1} = \lambda_n + \Delta\lambda, \tag{3}$$

where $\Delta\boldsymbol{u}$ and $\Delta\lambda$ are the increments of the nodal displacement vector and the load factor at the current step, $\boldsymbol{u}_n$ and λ_n represent their respective values at the previously converged load step.

After substituting the equations (2) and (3) into equation (1), the residual vector at the current load step can be written as:

$$\mathbf{R}(u_{n+1},\lambda_{n+1}) = \mathbf{F}_{\text{int}}(u_{n+1}) - \lambda_{n+1}\mathbf{F}_{\text{ext}} = 0. \tag{4}$$

To solve the under-determined system in equation (4), in the arc-length method, an additional equation, called as the arc-length equation, is proposed, which is given as [25–27]:

$$[\Delta u]^{\mathrm{T}}[\Delta u] + \psi[\Delta\lambda]^2\mathbf{F}_{\text{ext}}^{\mathrm{T}}\mathbf{F}_{\text{ext}} = [\Delta s]^2, \tag{5}$$

where s is the arc-length parameter, and Δs is its increment. The different arc-length schemes can be determined by adjusting the scalar parameter, ψ.

For a given Δs, (4) and (5)equations are solved by applying the Newton–Raphson scheme.

3.3. Finite Element Model. Based on FE software MSC. Marc, the initial FE models of the reversal process of the titanium diaphragms are developed, a representative FE mesh is shown in Figure 6. Due to the characteristics of axial symmetry, the preliminary FE mesh with 10240 regular solid shell elements is established. The thickness distributions of the diaphragms are implemented by a user subroutine. Figure 7 presents an example of a thickness model with range of 0.6 mm–0.9 mm and the corresponding FE model. The material properties for these simulations, including

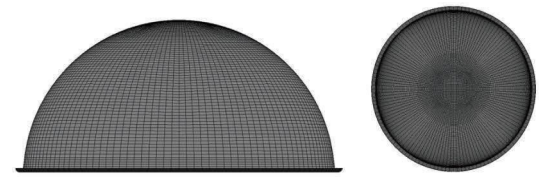

Figure 6: Preliminary FE mesh of the reversal process.

Young's modulus, Poisson's ratio, and density are 100 GPa, 0.34, and 4540 kg/m^3, respectively, and its plastic flow stress curve is shown in Figure 8. A face pressure is loaded on the outside surface of the FE mesh using the follower force function. All the nodes on the fillet edge are constrained in all directions.

4. Results and Discussion

4.1. Pressure Drop Characteristics and Model Verification. The relationships of pressure differential and apex axial displacement of two diaphragms are illustrated in Figure 9. It is clear that each of the curves change abruptly at two points, named critical point, such as A1 and A2, and overturning point, such as B1 and B2. The pressure differential at critical point refers to the critical pressure which begins to derive the deformation of the diaphragm. The one at the overturning point represents the overturning pressure which overturns the diaphragm completely. The simulated values of the critical pressure for the two diaphragms are 0.12 MPa and 0.097 MPa, respectively. The ones of overturning pressure are 0.55 MPa and 0.32 MPa. After the pressure exceeds the critical value, there are a local instable stage (LIS) and a stability stage (SS), and pressure differential changes slowly and apex axial displacement increases rapidly. In addition, the pressure differential displays an increasing tendency with the increase of apex axial displacement. This variation is related to the thickness distribution and the radial size of the diaphragm. The pressure differential gradient increases severely at the beginning of the reversal process because the arc segment of flanging gradually becomes straight.

In order to verify the simulated results, the comparisons between the simulated pressure differential data and experimental ones are also performed in these Figures. It is observed that the simulated results well agree with the experimental ones.

4.2. Effects of Structural Parameters on Pressure Differential. The relationships of pressure differential and apex axial displacement under different structural parameters can be obtained from the simulation results. The ones for the first group diaphragms are shown in Figure 10(a), and the ones for the diaphragms with the same thickness and chamfering radius but different bottom diameter and arc radius are shown in Figure 10(b). These curves have the same tendency but different local values. The critical pressure and the overturning pressure are observed obviously. It is found that the thickness, T, the bottom diameter, D_b, and the chamfering radius, R_f have effects on the critical

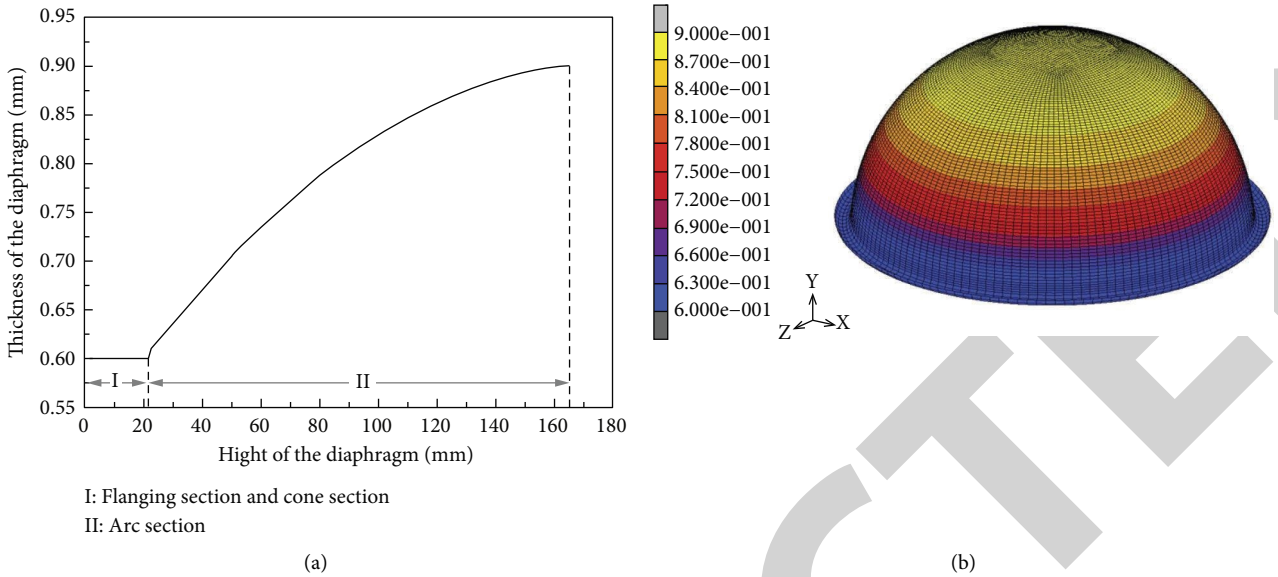

I: Flanging section and cone section
II: Arc section

(a) (b)

Figure 7: A thickness model (a) and the corresponding FE model (b).

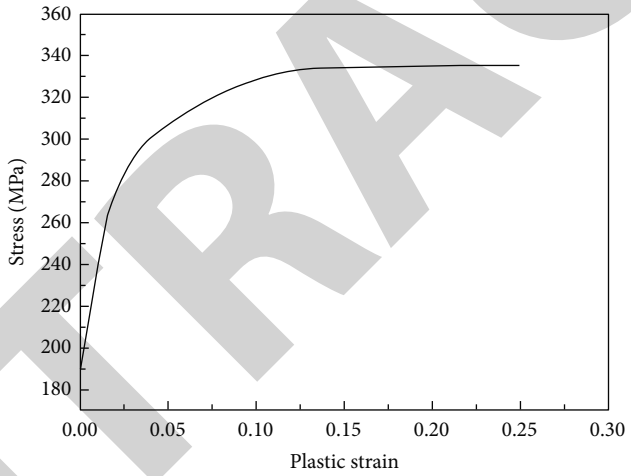

Figure 8: Plastic flow stress curve used in the FE model.

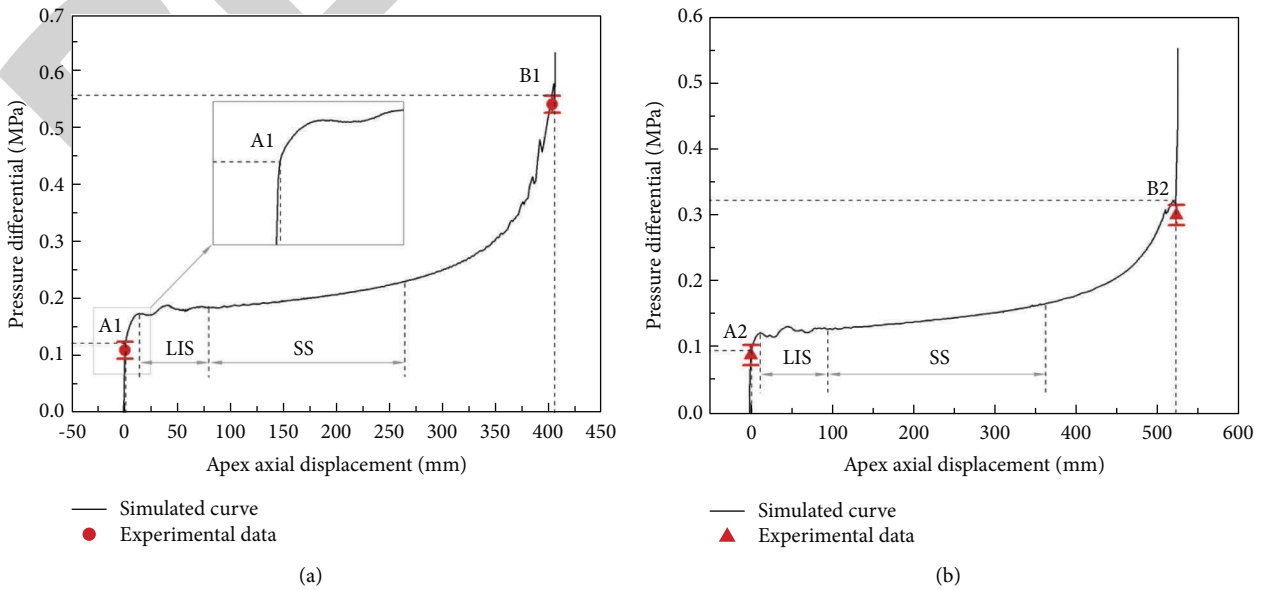

(a) (b)

Figure 9: Relationships of pressure differential and apex axial displacement of the diaphragms. (a) Serial number E1, (b) Serial number E2.

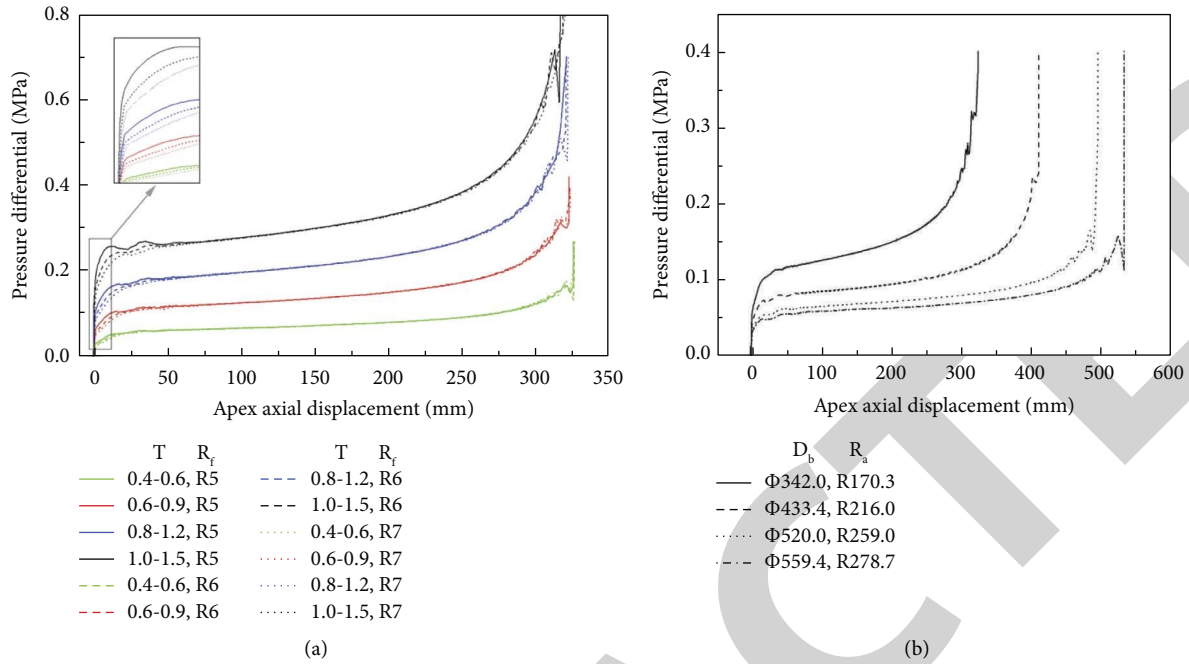

Figure 10: Relationships of pressure differential and apex axial displacement for the first group diaphragms (a); the diaphragms with same T and R_f (b).

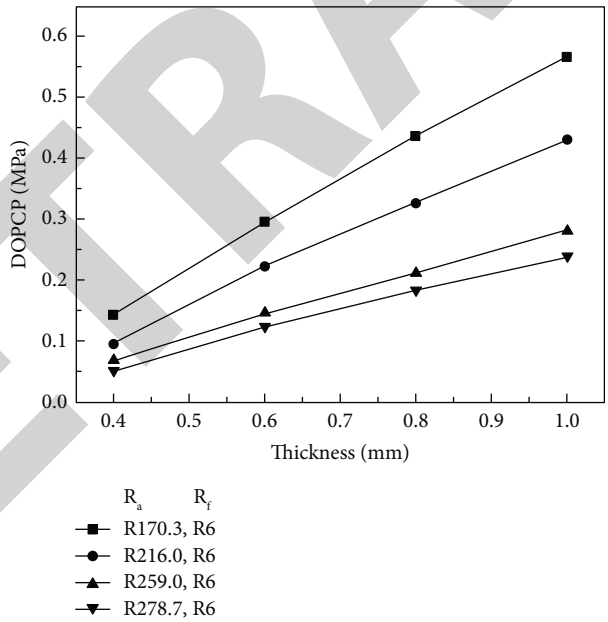

Figure 11: Variation of DOPCP and thickness.

pressure, and the effects of T and D_b are more significant. The overturning pressure is affected by the thickness, T, and the arc radius, R_a obviously.

In addition, the local instable phenomena become unclear with the decrease of the thickness. The differences of the overturning pressure and the critical pressure (DOPCP) increase with increasing thickness and decreasing arc radius as shown in Figure 11. The results indicate that the decrease of thickness leads to reducing the pressure differential, and further is beneficial to reducing the weight of the pressurizing system for titanium diaphragm tanks. However, if the thickness is too small, the structure of the diaphragm will become unstable. A polygon boundary is formed on the deformation position at the beginning of the reversal process, as shown in Figure 12(a). The strain localizations take place at the polygon vertexes, which will result in local cracks under poor pressure differential control.

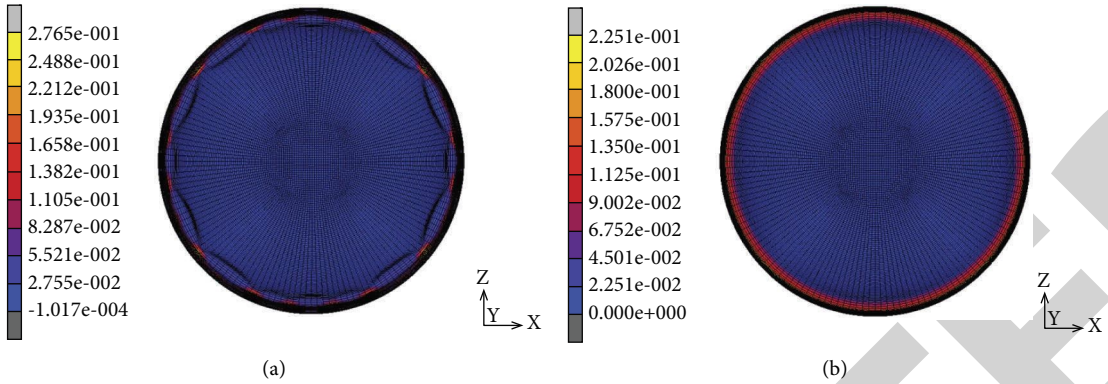

Figure 12: Comparisons of the shape and the plastic strain for the fourth group diaphragms. (a) Thickness: 0.4 mm–0.6 mm; (b) Thickness: 1.0 mm–1.5 mm.

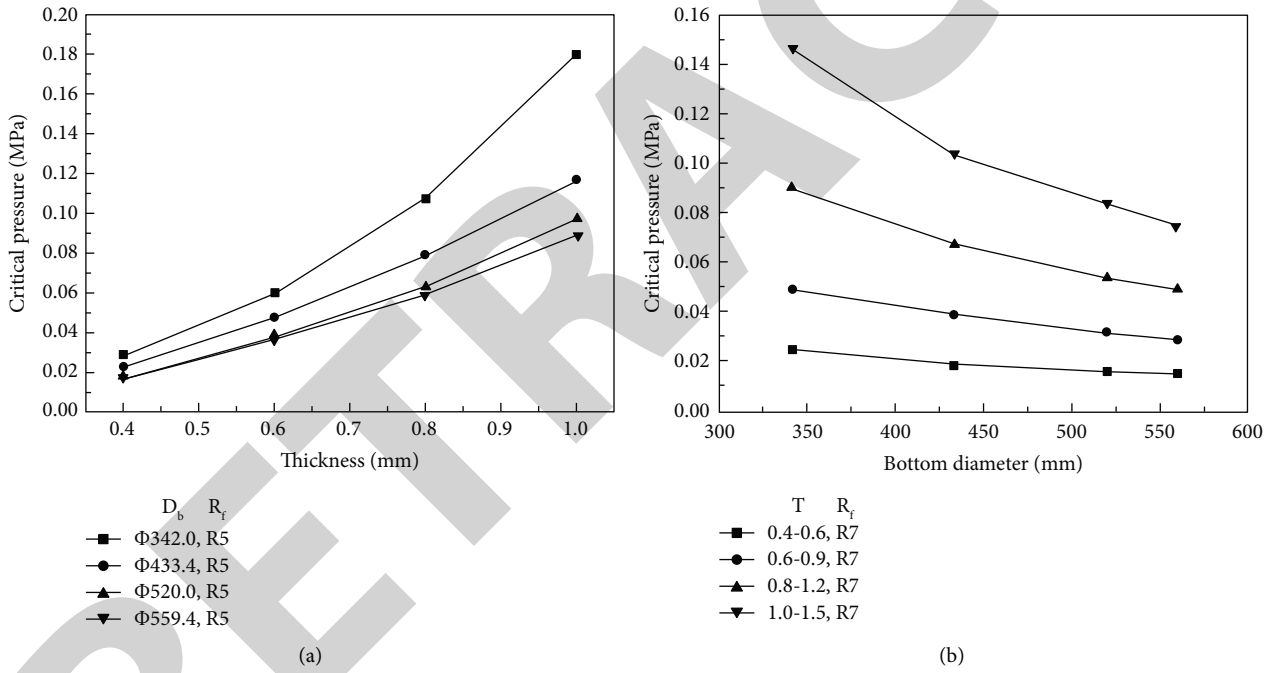

Figure 13: Continued.

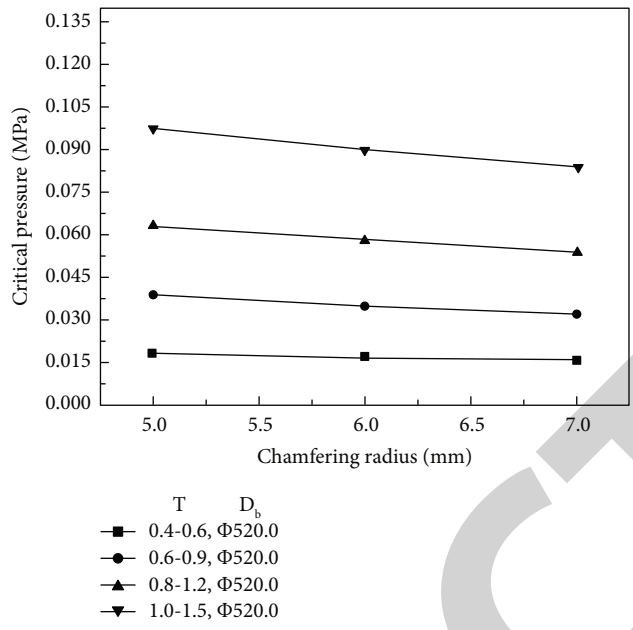

(c)

Figure 13: Effects of structural parameters on the critical pressure. (a) Thickness effects; (b) Bottom diameter effects; (c) Chamfering radius effects.

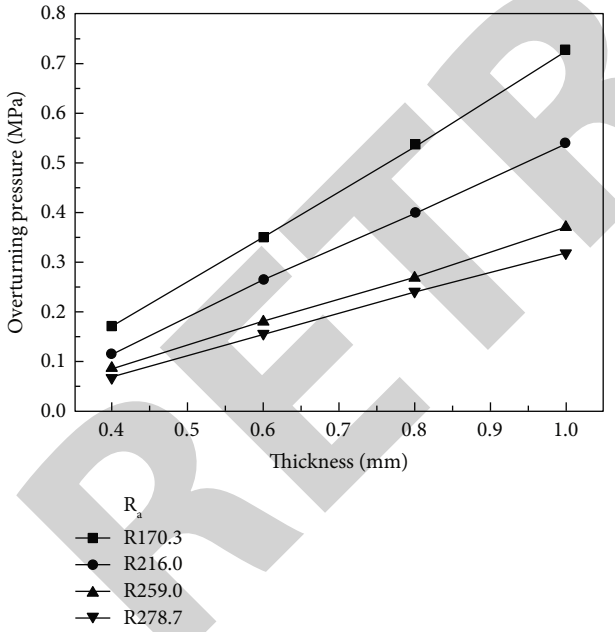

Figure 14: Effects of structural parameters on the overturning pressure.

The values of the critical pressure and the overturning pressure for every group are collected. The effects of the thickness, T, the bottom diameter, D_b, and the chamfering radius, R_f on the critical pressure are shown in Figure 13. The values of the critical pressure range from 0.015 MPa to 0.18 MPa. The equivalent von Mises stress at the deformed regions is larger than those in other regions. The maximum value is 249.5 MPa–266 MPa, which is far larger than the yield strength of TA1ELI. The increase of thickness, decreasing bottom diameter, and chamfering radius increase the deformation resistance of metal. So the critical pressure increases with the increasing thickness, decreasing bottom diameter and chamfering radius, and the thickness and the bottom diameter make the main contributions to the variation. Instead of the curve tendencies in Figure 13(c), nonlinear increases and decreases present in Figures 13(a) and 13(b), and these tendencies become sharper with increasing thickness. The effect of the thickness, T and the arc radius, R_a are shown in Figure 14. The values of the overturning pressure range from 0.07 MPa to 0.73 MPa. The overturning pressure increases with the increasing thickness and arc radius. It is interesting to notice that near-linear relationships between the overturning pressure and the thickness are remarkable. It is easy to predict the critical pressure and the overturning pressure by the above tendencies.

5. Conclusions

In this work, the effects of structural parameters on pressure differential to roll titanium diaphragms are investigated. The following conclusions have been drawn from the results of this investigation.

(1) The relationships of pressure differential and apex axial displacement of the diaphragms change abruptly at two points, including a critical point and an overturning point. After the pressure exceeds the critical value, there are a local instable stage and a

stability stage. Simulated values of the critical pressure and the overturning pressure show good agreement with measured ones.

(2) The local instable phenomena become unclear with the decrease of the thickness. The decrease of thickness is beneficial to reduce the weight of pressurizing system for titanium diaphragm tanks. If the thickness is too small, the strain localizations take place on the deformation position at the beginning of the reversal process, which will result in local cracks under poor pressure differential control.

(3) The critical pressure increases with increasing thickness, decreasing bottom diameter, and chamfering radius. The thickness and the bottom diameter are the main influence factors for the critical pressure. The overturning pressure increases with increasing thickness and arc radius. These effects of the bottom diameter, the chamfering radius, and arc radius become sharper with increasing thickness.

Data Availability

The data used to support the findings of the manuscript are included within this article.

Conflicts of Interest

The authors declare that they have no conflicts of interest.

Acknowledgments

The authors would like to express their gratitude to the financial support by the National Natural Science Foundation of China (Nos. 51801090).

References

[1] J. Vincent, J. M. Carella, and A. P. Cisilino, "Thermal analysis of the Girth Weld of an Elastomeric diaphragm tank," *Journal of Materials Processing Technology*, vol. 214, no. 2, pp. 428–435, 2014.

[2] B. Lenahen, S. Gangadharan, and M. Desai, "A computational and experimental analysis of spacecraft propellant tanks implemented with flexible diaphragms," in *54th AIAA/ASME/ASCE/AHS/ASC Structures, Structural Dynamics, and Materials Conference*Boston, Massachusetts, 2013.

[3] H. Zhang, S. D. Gu, J. J. Zhang et al., "Development of titanium diaphragms for Space propellant tank," in *Proceedings of the 2022 International Conference on Advanced Control*, Automation and Robotics, Guangzhou, China, March 2022.

[4] H. Sabaghzadeh and M. Shafaee, "Investigation of modal properties and Layout of Elastomer diaphragm tanks in Telecommunication Satellite," *Microsystem Technologies*, vol. 26, no. 6, pp. 1931–1959, 2020.

[5] D. Sances, S. Gangadharan, J. Sudermann, and B. Marsell, "CFD Fuel slosh modeling of Fluid-structure Interaction in spacecraft propellant tanks with diaphragms," in *51st AIAA/ASME/ASCE/AHS/ASC Structures, Structural Dynamics, and Materials Conference*Orlando, Florida, 2010.

[6] A. Leal-Junior, A. Frizera, and C. Marques, "A Fiber Bragg Gratings Pair Embedded in a Polyurethane diaphragm: towards a Temperature-insensitive pressure Sensor," *Optics & Laser Technology*, vol. 131, Article ID 106440, 2020.

[7] K. Anflo and R. Möllerberg, "Flight Demonstration of New Thruster and Green propellant Technology on the PRISMA Satellite," *Acta Astronautica*, vol. 65, no. 9-10, pp. 1238–1249, 2009.

[8] H. A. Conomos, C. G. Alongi, J. Moore et al., "Development of 10 inch diameter titanium rolling metal diaphragm tank for Green propellant," in *53rd AIAA/SAE/ASEE Joint Propulsion Conference*Atlanta Georgia, July 2017.

[9] I. Ballinger, W. Lay, and W. Tam, *Review and History of PSI Elastomeric Diaphragm Tanks*, (in English) American Institute of Aeronautics and Astronautics, Reston, Virginia, USA, 1995.

[10] X. Lei, Y. Deng, Z. Yin, and G. Xu, "Tungsten Inert gas and Friction Stir Welding characteristics of 4-mm-Thick 2219-T87 Plates at Room Temperature and -196°C," *Journal of Materials Engineering and Performance*, vol. 23, no. 6, pp. 2149–2158, 2014.

[11] B. Lenahen, A. Bernier, S. Gangadharan, J. Sudermann, and B. Marsell, "A computational investigation for determining the Natural Frequencies and Damping effects of diaphragm-implemented spacecraft propellant tanks," in *53rd AIAA/ASME/ASCE/AHS/ASC Structures, Structural Dynamics and Materials Conference*Honolulu Hawaii, April 2012.

[12] M. Marvih, H. Kammerer, and J. Gidley, *Parametric Evaluation of Contoured Aluminum Diaphragm, Positive Expulsion Tanks*, American Institute of Aeronautics and Astronautics, Reston, Virginia, USA, 1992.

[13] Q. Yang, R. Tao, and P. Wen, "Optimization design of Smart reversible diaphragms using shape Memory Polymer," in *Proceedings of the Advances in Structural and Multidisciplinary Optimization: Proceedings of the 17th World Congress of Structural and Multidisciplinary Optimization (WCSMO17)*, pp. 549–561, January 2018.

[14] S. Ding and F. G. Meng, "A Review on design method for storage tank of metal diaphragm with variable thickness," *J. Shenyang Inst. Aerona. Eng*, vol. 36, no. 2, pp. 9–14, 2019.

[15] S. Yuan, Z. C. Ma, X. L. Zhou, and Z. Liu, "Influence of thickness on Turning characteristics of a diaphragm in a titanium tank," *Mach. Tool Hydrau*, vol. 46, no. 11, pp. 135–139, 2018.

[16] F. Huang, T. Cheng, X. Q. Zhu, and Z. Liu, "Effect of Prebending radius of Flange on the Flipping behavior of the metal Tank's diaphragm," *Journal of Machine Design*, vol. 36, no. 4, pp. 45–48, 2019.

[17] H. F. Qiang, S. Zhou, X. R. Wang, and G. Wang, "Effect of angle on expulsion behavior of Spherical-cone metallic diaphragms for positive expulsion tanks," *Engineering Mechanics*, vol. 30, no. 4, pp. 435–441, 2013.

[18] J. Klatte, N. Darkow, R. Gajdacz, and S. Goek, "Sloshing and Pressurization tests for Membrane tank: tests, Validation and models," *Acta Astronautica*, vol. 175, pp. 338–348, 2020.

[19] A. Safdar, M. Islam, M. A. Akram, M. Mujahid, Y. Khalid, and S. I. Shah, "Reaction Time and Film thickness effects on Phase formation and Optical properties of solution processed Cu2ZnSnS4 thin Films," *Journal of Materials Engineering and Performance*, vol. 25, no. 2, pp. 457–465, 2016.

[20] N. Singh, S. Sharma, O. Parkash, and D. Kumar, "Synthesis and Characterization of Nanocrystalline Fe(100-x)Ni(x) alloy Powders by Auto-combustion and Hydrogen Reduction," *Journal of Materials Engineering and Performance*, vol. 28, no. 9, pp. 5441–5449, 2019.

[21] D. Žarković, Đ. Jovanović, V. Vukobratović, and Z. Brujić, "Convergence Improvement in computation of strain-softening solids by the arc-length method," *Finite Elements in Analysis and Design*, vol. 164, pp. 55–68, 2019.
[22] D. Bellora and R. Vescovini, "Hybrid Geometric-dissipative arc-length methods for the Quasi-static analysis of Delamination problems," *Computers & Structures*, vol. 175, pp. 123–133, 2016.
[23] C. Kadapa, "A Simple Extrapolated predictor for overcoming the Starting and Tracking issues in the arc-length method for nonlinear structural mechanics," *Engineering Structures*, vol. 234, no. 8, Article ID 111755, 2021.
[24] Y. Zhang, J. Huang, Y. Yuan, and H. A. Mang, "Cracking elements method with a Dissipation-based arc-length Approach," *Finite Elements in Analysis and Design*, vol. 195, Article ID 103573, 2021.
[25] G. A. Wempner, "Discrete approximations related to nonlinear Theories of solids," *International Journal of Solids and Structures*, vol. 7, no. 11, pp. 1581–1599, 1971.
[26] E. Riks, "An incremental Approach to the solution of Snapping and Buckling problems," *International Journal of Solids and Structures*, vol. 15, no. 7, pp. 529–551, 1979.
[27] M. A. Crisfield, "A Fast incremental/iterative solution procedure that Handles "Snap-through"," *Computers & Structures*, vol. 13, no. 1-3, pp. 55–62, 1981.